Ionic conductivity in a quantum lattice gas model with three-particle interactions

2012 J. Phys. A: Math. Theor. 45 494019

(http://iopscience.iop.org/1751-8121/45/49/494019)

J. Phys. A: Math. Theor. **45** (2012) 494019 (22pp) doi:10.1088/1751-8113/45/49/494019

Ionic conductivity in a quantum lattice gas model with three-particle interactions

J H Barry[1], **K A Muttalib**[1,3] **and T Tanaka**[2]

[1] Department of Physics, University of Florida, PO Box 118440, Gainesville, FL 32611-8440, USA
[2] Department of Physics and Astronomy, Ohio University, Athens, OH 45701, USA

E-mail: barry@phys.ufl.edu, muttalib@phys.ufl.edu and ttanaka@sannet.ne.jp

Received 14 May 2012, in final form 15 October 2012
Published 27 November 2012
Online at stacks.iop.org/JPhysA/45/494019

Abstract

A system of mesoscopic ions with dominant three-particle interactions is modeled by a quantum lattice liquid on the planar kagomé lattice. The two-parameter Hamiltonian contains localized attractive triplet interactions as potential energy and nearest neighbor hopping-type terms as kinetic energy. The dynamic ionic conductivity $\sigma(\omega)$ is theoretically investigated for 'weak hopping' via a quantum many-body perturbation expansion of the thermal (Matsubara) Green function (current-current correlation). A simple analytic continuation and mapping of the thermal Green function provide the temporal Fourier transform of the physical retarded Green function in the Kubo formula. Substituting pertinent exact solutions for static multi-particle correlations known from previous work, Arrhenius relations are revealed in zeroth-order approximation for the dc ionic conductivity σ_{dc} along special trajectories in density–temperature space. The Arrhenius plots directly yield static activation energies along the latter loci. Experimental possibilities relating to σ_{dc} are discussed in the presence of equilibrium aggregation.

This article is part of 'Lattice models and integrability', a special issue of *Journal of Physics A: Mathematical and Theoretical* in honour of F Y Wu's 80th birthday.

PACS numbers: 66.10.Ed, 82.70.Dd

(Some figures may appear in colour only in the online journal)

1. Introduction

It is a pleasure to honor F Y (Fred) Wu on the occasion of his 80th birthday. His outstanding contributions to the theory of exactly soluble models in statistical physics and to multiple mathematical fields are commendable. Wu's incisive reasonings and lucid writing are valued by researchers with varied interests. The present paper on dynamic ionic conductivity is a

[3] Author to whom any correspondence should be addressed.

case in point. The perturbation theory demonstrates that exact solutions for thermodynamic (static) multiparticle correlations in the unperturbed system are needed to evaluate the Kubo formula of linear response theory. To determine such correlations, the authors made *a priori* use [1] of requisite results by Wu [2] connecting the partition functions of a generalized (three-parameter) kagomé Ising model and a standard (two-parameter) honeycomb Ising model, with an eight-vertex model playing a mediating role. Vintage Fred Wu!

Theoretical studies of strongly correlated systems in condensed matter physics primarily consider two-particle interactions. However, particularly at higher densities, multiparticle interactions can be germane and lead to significant effects. Examples include ring-exchange processes in the nuclear magnetism of He^3 [3], four-spin interactions in undoped high-T_c compounds and cuprate ladders [4], and three-particle exchanges in a system of two atomic species embedded in a frustrated optical lattice [5]. Regarding dominance between pair and multiparticle interactions, it is noteworthy that ultracold gases of polar molecules on an optical lattice can be tuned to possess *purely* three-particle interactions [6]. Additional examples of many-body interactions involve electron screening in metals [7], island formation on surfaces [8], chemical processes in solids [9] and various other illustrations.

Notwithstanding, direct experimental measurements of multiparticle interactions among the microscopic constituents in condensed matter are typically unattainable since the actual trajectories of the microscopic particles in space and time cannot be measured to provide the necessary positional information. In contrast, the pertinent scales (size, mass, charge, ...) in, e.g., colloidal suspensions are 'mesoscopic' and the individual colloidal particle trajectories are accessible using optical experiments. For instance, three-particle interactions among colloidal particles can be directly measured on *optical lattices* whose sites are 'optical traps' for the mesoscopic particles and 'optical tweezers' can configure the colloidal particles as needed [10]. More specifically, three-body interactions have been measured among three charged colloidal particles in a deionized solvent, and their triplet interaction was determined to be *attractive* and comparable in strength and range to their pair interactions. Numerical nonlinear Poisson–Boltzmann calculations show good agreement with the experimental results. Additionally, by changing the salinity of the solvent, the pair Yukawa (exponentially screened) potential between ions can be varied over a wide range, e.g., from short-ranged steric to long-ranged electrostatic or dipole–dipole.

Our research is motivated in part by experiments in the Konstanz–Stuttgart group [10], where the mesoscopic system consists of one micron diameter charged silica spheres suspended in saline water, each carrying an effective electric charge $q = 6500\ e$. Tuning the salinity *screens* the electrostatic repulsive pair interactions between spheres and their attractive three-particle interactions become directly measurable. These experiments upon a particular mesoscopic system are the first *direct* measurements of the three-particle interactions. Hence, theoretical investigations of the system offer opportunities to examine the effects of three-body attractive interactions on transport in contrast to the typical repulsive pair interactions. A colloidal system having dominant attractive interactions can experience *equilibrium aggregation* (condensation) of the colloidal ions into clusters on scales of several microns [11]. The condensation occurs when the thermal energy $kT \lesssim |U|$, where $|U|$ is the strength parameter of the attractive interaction. The present theory calculates the dynamic ionic conductivity $\sigma(\omega)$ in the *presence* of the phase transitions and critical behavior. The concurrence or interplay of transport and aggregation phenomena is itself a challenging problem in the statistical theory of complex fluids and the added experimental possibilities make the problem even more engaging. The usual scattering of the mesoscopic ions with the microscopic molecules of the solvent is not included directly in the present theory. This contribution can be incorporated *a posteriori* by comparison with experiments.

If a continuum ionic fluid system is discretized (or 'latticized'), the ionic conductivity is often described as a diffusion process wherein the ions 'hop' from site to site as they traverse the specimen. Since the ions are mesoscopically large objects, they may be treated as classical particles whose variables commute on *different* lattice sites (bosonic character). However, due to their large size, no more than one of these mobile ions can simultaneously appear on the same lattice site, which is an exclusion principle that can be represented by anticommutation relations on the *same* site (fermionic character). Using the *mixed* operator algebra, we consider a two-parameter *quantum lattice gas* (QLG) model with localized three-particle interactions on a planar kagomé lattice. More specifically, the potential energy in the QLG Hamiltonian contains *attractive triplet* interactions around each triangular face of the kagomé lattice, and the kinetic energy contains nearest-neighbor hopping terms along the lattice bonds. Historically, the QLG model Hamiltonian with nearest-neighbor pair attractive interactions was introduced by Matsubara and Matsuda [12] as a lattice liquid model for He^4 (hard-core Bose fluid). Special attention is also directed to the QLG model with nearest-neighbor pair repulsive interactions applied to ionic conductivity by Mahan [13], and by Tanaka *et al* [14] with application to the honeycomb layered superionic conductor $AgCrS_2$.

The method employed to theoretically examine ionic conductivity in the present QLG model develops a quantum many-body perturbation expansion of a thermal (Matsubara) Green function [15] (current–current correlation). The perturbation development assumes that $t_0 \ll |U|$ ('weak hopping'), where t_0 ($|U|$) is the strength parameter of the kinetic (potential) energy in the QLG model. The thermal (Matsubara) Green function is chosen since it has the mathematical advantage of leading directly to the physical retarded Green function and has simple S-matrix properties suitable for higher orders in the perturbation expansion. The ionic conductivity will be calculated via the Kubo formula, more particularly, the frequency dependent conductivity $\sigma(\omega)$ is obtained from the imaginary part of the Fourier transform of the two-time retarded Green function which in turn is found from a simple analytic continuation and mapping of the Matsubara Green function. As results, Arrhenius relations are revealed in zeroth-order approximation for the dc ionic conductivity along both the 'liquid' and 'vapor' branches of the unperturbed system coexistence curve (except in close proximity to the critical point) and along the continuation of its curvilinear diameter into the disordered fluid region (except in close proximity to full occupancy of the lattice). The Arrhenius plots directly yield *static activation energies* of the charged colloidal system along the above trajectories in density–temperature space. Experimental considerations relating to σ_{dc} are discussed in the presence of the above equilibrium aggregation.

The paper is organized as follows. Section 2 presents the QLG model and section 3 calculates its ionic current operator $\mathcal{J}$. Section 4 then obtains the general form of the thermal (Matsubara) Green function and its perturbation expansion is developed in powers of t_0 by means of a scattering operator. Section 5 applies the perturbation formalism in zeroth-order approximation (single-ion uncorrelated hops) which section 6 expresses in terms of known [1] thermodynamic (static) multi-particle correlations of the unperturbed system. Section 7 derives the initial dynamic ionic conductivity $\sigma(\omega)$ whose static limit provides the dc conductivity σ_{dc}. Section 8 uses the dc results to construct its Arrhenius plots yielding static activation energies of the colloidal ion system along select loci in density–temperature space. Section 9 considers experimental possibilities relating to σ_{dc}. Section 10 is a summary and discussion.

2. Quantum lattice-gas model having attractive triplet interactions

One considers a two-dimensional kagomé lattice (figure 1) with colloidal ions participating in the ionic transport. These mobile ions are described by a quantum lattice-gas (QLG)

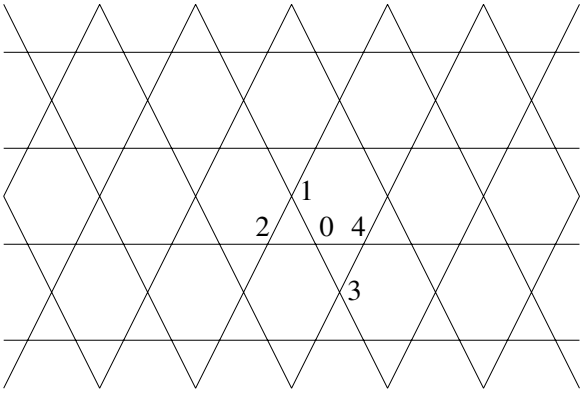

Figure 1. Diagram showing a kagomé lattice, which is a regular (all sites equivalent, all bonds equivalent) two-dimensional periodic array of equilateral triangles and regular hexagons with a coordination number 4. The origin site and its four nearest neighboring sites are specifically enumerated. Whenever three colloidal particles of the lattice liquid simultaneously occupy the vertices of an elementary triangle (say sites 0, 1, 2), these particles experience a triplet attractive interaction with strength parameter $|U|$.

Hamiltonian

$$\begin{aligned}\mathcal{H} &= \mathcal{H}_0 + \mathcal{H}_1 \\ &= U \sum_{<i,j,k>} n_i n_j n_k + t_0 \sum_{i,\delta} a^\dagger_{i+\delta} a_i \end{aligned} \tag{1}$$

where $\mathcal{H}_0$ is a potential energy form for a classical lattice gas having three-particle attractive interactions ($U < 0$) around each triangular face of the kagomé lattice, with $n_i \equiv a^\dagger_i a_i$ being an idempotent site-occupation number and $\sum_{\langle i,j,k\rangle}$ denotes summation over all elementary triangles of the lattice. The kinetic energy form $\mathcal{H}_1$ has a 'hopping integral' strength parameter $t_0 > 0$, and δ represents a nearest-neighbor site of site i. In the forthcoming perturbation analyses, $t_0 \ll |U|$ ('weak hopping') is assumed. A portion of the kagomé lattice is shown in figure 2, where the edge length $d \equiv |\vec{\delta_l}|$ of the lattice is a nearest-neighbor 'jump' distance along the crystallographic axes.

As mentioned earlier, the model (1) utilizes 'mixed statistics' in which the particles behave like bosons on different sites but as fermions on the same site. The QLG operator algebra is thus equivalent to the Pauli spin 1/2 operator algebra, and is expressed by the commutation relations

$$\left[a^\dagger_i, a^\dagger_j\right] = [a_i, a_j] = \left[a_i, a^\dagger_j\right] = 0, \quad i \neq j \tag{2a}$$

and the anticommutation relations

$$\left\{a^\dagger_i, a^\dagger_i\right\} = \{a_i, a_i\} = 0; \qquad \left\{a_i, a^\dagger_i\right\} = 1. \tag{2b}$$

The kagomé lattice is chosen for three reasons. First, the lattice is regular, and a regular lattice is favored to discretize configurational continuum space. Secondly, the lattice is 'close-packed', i.e. contains triangles, thereby accommodating the highly-localized triplet interactions under consideration. Third, the lattice is the only regular planar lattice for which the needed *exact solutions* are known. However, since the interactions are attractive, one can surmise that similar qualitative results would emerge if the desired exact solutions were available on the triangular lattice, the only other close-packed regular lattice in two-dimensions.

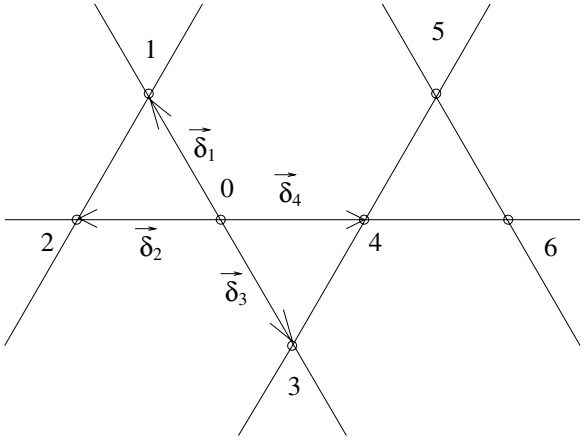

Figure 2. A portion of the kagomé lattice containing seven sites $0, 1, \ldots, 6$ for later use. An arbitrary origin site 0 has four nearest-neighbor vectors $\vec{\delta_l}$, where the nearest neighbor 'jump distance' $d = |\vec{\delta_l}|$, $l = 1, 2, 3, 4$. Local lattice inversion symmetry is manifest through the relations $\vec{\delta_1} = -\vec{\delta_3}$, and $\vec{\delta_2} = -\vec{\delta_4}$.

3. The ionic current operator $\mathcal{J}$

The *ionic polarization* operator $\mathcal{P}$ of the colloidal ion system is defined by

$$\mathcal{P} = q \sum_i n_i \vec{r}_i, \tag{3}$$

where $q > 0$ is the ionic electric charge and $\vec{r}_i$ is the lattice position vector of site i. The *ionic current operator* $\mathcal{J}$ of the system is then found as

$$\begin{aligned}
\mathcal{J} = \dot{\mathcal{P}} &= \frac{\mathrm{i}}{\hbar}[\mathcal{H}, \mathcal{P}] \\
&= \frac{\mathrm{i}q}{\hbar}\left[\mathcal{H}_0 + \mathcal{H}_1, \sum_j n_j \vec{r}_j\right] \\
&= \frac{\mathrm{i}q}{\hbar}\left[\mathcal{H}_0, \sum_j n_j \vec{r}_j\right] + \frac{\mathrm{i}q}{\hbar}\left[\mathcal{H}_1, \sum_j n_j \vec{r}_j\right] \\
&= -\frac{\mathrm{i}qt_0}{\hbar} \sum_{i,\delta} \sum_j \vec{r}_j \left[n_j, a^\dagger_{i+\delta} a_i\right] \\
&= -\frac{\mathrm{i}qt_0}{\hbar} \sum_{i,\delta} a^\dagger_{i+\delta} a_i \vec{\delta}_{i\delta}, \qquad \vec{\delta}_{i\delta} \equiv \vec{r}_{i+\delta} - \vec{r}_i,
\end{aligned} \tag{4}$$

where the Hamiltonian operator (1) and the ionic polarization operator (3) have been substituted. In the above operator algebra, direct use was made of the fact that the commutator $[\mathcal{H}_0, \sum_j n_j \vec{r}_j]$ vanishes, and the ensuing calculations were accomplished through recurrent use of the familiar commutator identity $[A, BC] = [A, B]C + B[A, C]$ and the mixed operator algebra (2).

4. The Matsubara Green function: perturbation expansion in powers of t_0

Rather than the physical double-time retarded Green function, the thermal (Matsubara) Green function is selected since it has the mathematical convenience of leading directly to the physical retarded Green function and has simple S-matrix properties suitable for higher orders in the perturbation development. The ionic conductivity will be calculated by means of the Kubo formula, more specifically, the frequency-dependent conductivity $\sigma(\omega)$ is procured from the imaginary part of the Fourier transform of the two-time retarded Green function which in turn is found from a simple analytic continuation and mapping of the Matsubara Green function.

Since the theory will employ the grand canonical ensemble, one introduces, in the usual manner,

$$\begin{aligned} H &\equiv \mathcal{H} - \mu N \\ &= \mathcal{H}_0 + \mathcal{H}_1 - \mu \sum_{i=1}^{\mathcal{N}} n_i, \end{aligned} \tag{5}$$

with μ being the chemical potential of the colloidal ion species and $N(= \sum_{i=1}^{\mathcal{N}} n_i)$ the conjugate total number operator where $\mathcal{N}$ is the total number of lattice sites. For notational and calculational convenience, one incorporates the chemical potential term into the symbol $\mathcal{H}_0$ for the unperturbed Hamiltonian, i.e.

$$H = \mathcal{H}_0 + \mathcal{H}_1 \tag{6a}$$

where

$$\mathcal{H}_0 = U \sum_{<i,j,k>} n_i n_j n_k - \mu \sum_{i=1}^{\mathcal{N}} n_i; \quad \mathcal{H}_1 = t_0 \sum_{i,\delta} a^\dagger_{i+\delta} a_i, \tag{6b}$$

having explicitly entered (1).

The *thermal (Matsubara) Green function* $\Pi(\tau)$ is defined by [13]

$$\Pi(\tau) \equiv \tfrac{1}{2} \langle T_\tau \mathcal{J}(\tau) \cdot \mathcal{J}(0) \rangle_H \tag{7a}$$

where

$$\langle \cdots \rangle_H \equiv \mathrm{Tr}(\mathrm{e}^{-\beta H} \cdots)/\mathrm{Tr}\ \mathrm{e}^{-\beta H} \tag{7b}$$

and

$$\mathcal{J}(\tau) \equiv \mathrm{e}^{\tau H} \mathcal{J}(0)\, \mathrm{e}^{-\tau H} \tag{7c}$$

is the ionic current operator in the (τ-shifted) '*thermal' Heisenberg representation*, T_τ is the *τ-ordering operator* (larger τs stand to the left), and $\beta = 1/kT$ with k being the Boltzmann constant and T the absolute temperature. Since τ is real with domain $-\beta \leqslant \tau \leqslant \beta$, one notes that the thermal Heisenberg operator $\mathcal{J}(\tau)$ is non-Hermitian in contrast to a usual (time-shifted) Heisenberg operator $\mathcal{J}(t)$.

Using (4) and (7*a*), one obtains

$$\begin{aligned} \Pi(\tau) &= \frac{1}{2} \langle T_\tau \mathcal{J}(\tau) \cdot \mathcal{J}(0) \rangle_H \\ &= -\frac{1}{2} \left(\frac{q t_0}{\hbar} \right)^2 \sum_{i,j,\delta,\delta'} (\vec{\delta}_{i\delta} \cdot \vec{\delta}_{j\delta'}) \langle T_\tau a^\dagger_{j+\delta'}(\tau) a_j(\tau) a^\dagger_{i+\delta}(0) a_i(0) \rangle_H \\ &= -\frac{1}{2} \left(\frac{q t_0}{\hbar} \right)^2 \sum_{i,j,\delta,\delta'} (\vec{\delta}_{i\delta} \cdot \vec{\delta}_{j\delta'}) \frac{1}{2} (\langle T_\tau a^\dagger_{j+\delta'}(\tau) a_j(\tau) a^\dagger_{i+\delta} a_i \rangle_H + \langle \mathrm{h.c.} \rangle_H). \end{aligned} \tag{8}$$

The quantum many-body perturbation expansion of (8) in powers of t_0 is engendered by utilizing a scattering operator. Specifically, the thermal average within the summand of (8) is now written as

$$\langle T_\tau[a^\dagger_{j+\delta'}(\tau)a_j(\tau)a^\dagger_{i+\delta}(0)a_i(0)]\rangle_H = \langle T_\tau[S(\beta)a^\dagger_{j+\delta'}(\tau)a_j(\tau)a^\dagger_{i+\delta}(0)a_i(0)]\rangle_{\mathcal{H}_0}/\langle S(\beta)\rangle_{\mathcal{H}_0} \quad (9a)$$

where

$$\mathrm{e}^{-\beta H} = \mathrm{e}^{-\beta\mathcal{H}_0}S(\beta) \quad (9b)$$

with the *scattering operator* [15]

$$S(\beta) \equiv T_\tau[\mathrm{e}^{-\int_0^\beta \mathcal{H}_1(\tau_1)\mathrm{d}\tau_1}]. \quad (9c)$$

On the right-hand side of (9), the notations mean:

$$\begin{aligned}
&\langle\cdots\rangle_{\mathcal{H}_0} = \mathrm{Tr}(\mathrm{e}^{-\beta\mathcal{H}_0}\cdots)/\mathrm{Tr}\,\mathrm{e}^{-\beta\mathcal{H}_0}\\
&a(\tau) = \mathrm{e}^{\tau\mathcal{H}_0}a\,\mathrm{e}^{-\tau\mathcal{H}_0} \qquad (10a)\\
&a^\dagger(\tau) = \mathrm{e}^{\tau\mathcal{H}_0}a^\dagger\,\mathrm{e}^{-\tau\mathcal{H}_0} \neq (a(\tau))^\dagger\\
&\mathcal{H}_1(\tau) = \mathrm{e}^{\tau\mathcal{H}_0}\mathcal{H}_1\,\mathrm{e}^{-\tau\mathcal{H}_0}\\
&\qquad = t_0\sum_{k,\delta''}\mathrm{e}^{\tau\mathcal{H}_0}a^\dagger_{k+\delta''}a_k\,\mathrm{e}^{-\tau\mathcal{H}_0}\\
&\qquad = t_0\sum_{k,\delta''}\mathrm{e}^{\tau\mathcal{H}_0}a^\dagger_{k+\delta''}\,\mathrm{e}^{-\tau\mathcal{H}_0}\,\mathrm{e}^{\tau\mathcal{H}_0}a_k\,\mathrm{e}^{-\tau\mathcal{H}_0}\\
&\qquad = t_0\sum_{k,\delta''}a^\dagger_{k+\delta''}(\tau)a_k(\tau), \qquad (10b)
\end{aligned}$$

having initially substituted the $\mathcal{H}_1$ expression (6*b*). The (10) operators $a(\tau)$, $a^\dagger(\tau)$, $\mathcal{H}_1(\tau)$ are now said to be in the *thermal interaction representation*. One also notes that the rhs ratio expression in (9*a*) contains solely unperturbed thermal averages.

The scattering operator $S(\beta)$ in (9*c*) may be developed in powers of t_0 as

$$S(\beta) = T_\tau\left[1 - t_0\sum_{k,\delta''}\int_0^\beta \mathrm{d}\tau_1 a^\dagger_{k+\delta''}(\tau_1)a_k(\tau_1) + o\big(t_0^2\big)\right] \quad (11)$$

where (10*b*) has been substituted. Expression (11) is then itself substituted into (9*a*) yielding for the numerator

$$\begin{aligned}
\langle T_\tau[S(\beta)a^\dagger_{j+\delta'}(\tau)a_j(\tau)a^\dagger_{i+\delta}(0)a_i(0)]\rangle_0 &= \langle T_\tau[a^\dagger_{j+\delta'}(\tau)a_j(\tau)a^\dagger_{i+\delta}(0)a_i(0)]\rangle_0\\
&- t_0\sum_{k,\delta''}\int_0^\beta \mathrm{d}\tau_1\langle T_\tau[a^\dagger_{k+\delta''}(\tau_1)a_k(\tau_1)a^\dagger_{j+\delta'}(\tau)a_j(\tau)a^\dagger_{i+\delta}(0)a_i(0)]\rangle_0 + o\big(t_0^2\big)
\end{aligned} \quad (12a)$$

and for the denominator

$$\langle S(\beta)\rangle_0 = 1 - t_0\sum_{k,\delta''}\int_0^\beta \mathrm{d}\tau_1\langle T_\tau a^\dagger_{k+\delta''}(\tau_1)a_k(\tau_1)\rangle_0 + o\big(t_0^2\big). \quad (12b)$$

For notational brevity, the subscript $\mathcal{H}_0$ on thermal averages in (9*a*) has been subsequently replaced by the subscript 0.

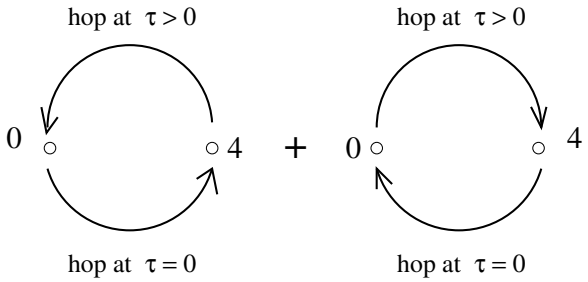

Figure 3. A diagrammatic representation of expression (15), where τ increases upward. Upon summation in (8), each non-vanishing term from (13) may be represented by a nearest-neighbor closed directed diagram returning to its $\tau = 0$ starting point.

5. Reduction of the Matsubara Green function in zeroth-order approximation

Using (12), the zeroth-order approximation (single-ion uncorrelated hops) in the perturbation expansion of (9*a*) becomes

$$\langle T_\tau[S(\beta)a^\dagger_{j+\delta'}(\tau)a_j(\tau)a^\dagger_{i+\delta}(0)a_i(0)]\rangle_H = \langle T_\tau[a^\dagger_{j+\delta'}(\tau)a_j(\tau)a^\dagger_{i+\delta}(0)a_i(0)]\rangle_0 + o(t_0), \tag{13}$$

where one has employed the fact that the (12*b*) denominator expression $\langle S(\beta)\rangle_0 = 1 + o(t_0^2)$ since the thermal average $\langle a^\dagger_{k+\delta''}(\tau_1)a_k(\tau_1)\rangle_0 \equiv 0$. The latter null result can be proven by first writing

$$\langle a^\dagger_{k+\delta''}(\tau_1)a_k(\tau_1)\rangle_0 = \mathrm{Tr}\big(\mathrm{e}^{-\beta\mathcal{H}_0}\mathrm{a}^\dagger_{\mathrm{k}+\delta''}(\tau_1)\mathrm{a}_\mathrm{k}(\tau_1)\big)\big/\mathrm{Tr}\ \mathrm{e}^{-\beta\mathcal{H}_0}, \tag{14}$$

and using a product representation in which $\mathcal{H}_0$ is diagonal, one argues (see section 6) that $\mathrm{e}^{-\beta\mathcal{H}_0}a^\dagger_{k+\delta''}(\tau_1)a_k(\tau_1)$ is purely off-diagonal and thus traceless.

As used shortly, the zeroth-order approximation expression (13) leads solely, upon summation in (8), to two companion clusters for *each* distinct nearest neighbor bond $\langle i, j\rangle$. For example, associated with the $\langle 0, 4\rangle$ bond in figures 1 and 2, one has

$$\langle a^\dagger_0(\tau)a_4(\tau)a^\dagger_4(0)a_0(0)\rangle_0 + \langle a^\dagger_4(\tau)a_0(\tau)a^\dagger_0(0)a_4(0)\rangle_0. \tag{15}$$

Each term in (15) has an obvious physical 'hopping' interpretation; for instance, $\langle a^\dagger_0(\tau)a_4(\tau)a^\dagger_4(0)a_0(0)]\rangle_0$ corresponds to an ion being destroyed at origin site 0 at $\tau = 0$ and created at site 4 at $\tau = 0$, followed by an ion being destroyed at site 4 at $\tau > 0$ and created at the origin site 0 at the same $\tau > 0$. A diagrammatic representation of (15) is seen in figure 3.

Hence, substituting (13) into (8), the Matsubara Green function becomes in zeroth-order approximation:

$$\begin{aligned}
\Pi(\tau) &= \frac{1}{2}\langle T_\tau \mathcal{J}(\tau)\cdot\mathcal{J}(0)\rangle_H \\
&= -\frac{1}{2}\left(\frac{qt_0}{\hbar}\right)^2 \sum_{i,j,\delta,\delta'} (\vec{\delta}_{i\delta}\cdot\vec{\delta}_{j\delta'})\frac{1}{2}(\langle T_\tau[a^\dagger_{j+\delta'}(\tau)a_j(\tau)a^\dagger_{i+\delta}(0)a_i(0)\rangle_0 + \langle\mathrm{h.c.}\rangle_0]) + o(t_0^3) \\
&= -\frac{1}{2}\left(\frac{qt_0}{\hbar}\right)^2 (-d^2)\frac{\mathcal{N}\tilde{z}}{2}(\langle a^\dagger_0(\tau)a_4(\tau)a^\dagger_4(0)a_0(0)]\rangle_0 \\
&\quad + \langle a^\dagger_4(\tau)a_0(\tau)a^\dagger_0(0)a_4(0)]\rangle_0) + o(t_0^3) \\
&= \frac{\mathcal{N}\tilde{z}}{2}\left(\frac{qt_0 d}{\hbar}\right)^2 M(\tau) + o(t_0^3),
\end{aligned} \tag{16a}$$

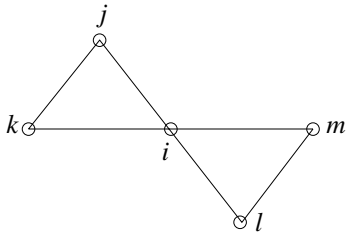

Figure 4. A kagomé lattice site i and its nearest neighbor sites j, k, l, m.

where, in particular, $\vec{\delta}_{i\delta} \cdot \vec{\delta}_{j\delta'} = (\vec{r}_{i+\delta} - \vec{r}_i) \cdot (\vec{r}_{j+\delta'} - \vec{r}_j) \to (\vec{r}_4 - \vec{r}_0) \cdot (\vec{r}_0 - \vec{r}_4) = -d^2$, with d being the edge length (nearest-neighbor 'jump' distance) of the lattice, $\mathcal{N}\tilde{z}/2$ is the number of nearest neighbor bonds with $\tilde{z}$ being the coordination number of the kagomé lattice, and

$$M(\tau) \equiv \tfrac{1}{2}(\langle a_0^\dagger(\tau)a_4(\tau)a_4^\dagger(0)a_0(0)]\rangle_0 + \langle a_4^\dagger(\tau)a_0(\tau)a_0^\dagger(0)a_4(0)]\rangle_0). \tag{16b}$$

6. Evaluation of the Matsubara Green function in zeroth-order approximation

In order to evaluate the unperturbed thermal averages in $M(\tau)$ equation (16*b*), it will be convenient to first state three rules. The rules have been established [14] by employing a complete orthonormal set $\{|n_0\rangle|n_1\rangle \cdots |n_{r-1}\rangle\}$ of eigen-functions of the unperturbed Hamiltonian $\mathcal{H}_0$ along with (2) and standard use of the single-site operator relations

$$\begin{aligned} &n_i^{op}|n_i\rangle = n_i|n_i\rangle, \qquad n_i = 0, 1 \\ &a_i^\dagger|1\rangle = 0; \qquad a_i^\dagger|0\rangle = |1\rangle; \\ &a_i|0\rangle = 0; \qquad a_i|1\rangle = |0\rangle, \end{aligned} \tag{17}$$

where the single-site occupation number operator $n_i^{\rm op} = a_i^\dagger a_i$.

The localized site-labels in figure 4 are used in the statement of the rules.

Rule 1.

$$\begin{aligned} a_i^\dagger(\tau) &= \mathrm{e}^{\tau\mathcal{H}_0} a_i^\dagger \,\mathrm{e}^{-\tau\mathcal{H}_0} = \mathrm{e}^{\tau U(n_j n_k + n_l n_m) - \tau\mu} a_i^\dagger \\ a_i(\tau) &= \mathrm{e}^{\tau\mathcal{H}_0} a_i \,\mathrm{e}^{-\tau\mathcal{H}_0} = \mathrm{e}^{-\tau U(n_j n_k + n_l n_m) + \tau\mu} a_i, \end{aligned} \tag{18}$$

where the $\mathcal{H}_0$ expression (6b) has been substituted and the site labels in figure 4 were entered.

Rule 2.

For any analytic function $f(n_i)$, one finds

$$a_i^\dagger f(n_i) = f(0)a_i^\dagger; \qquad f(n_i)a_i^\dagger = f(1)a_i^\dagger; \tag{19a}$$

$$a_i f(n_i) = f(1)a_i; \qquad f(n_i)a_i = f(0)a_i. \tag{19b}$$

Rule 3.

The exponential operator e^{un_i} can be expressed in terms of projection operators n_i, $1 - n_i$:

$$\mathrm{e}^{un_i} = (1 - n_i) + n_i\,\mathrm{e}^u. \tag{20}$$

Now, as needed in (16*b*) with its figure 2 site-labels, one obtains

$$\begin{aligned} 2M(\tau) &= \langle a_0^\dagger(\tau)a_4(\tau)a_4^\dagger(0)a_0(0)]\rangle_0 + \langle a_4^\dagger(\tau)a_0(\tau)a_0^\dagger(0)a_4(0)]\rangle_0 \\ &= \langle \mathrm{e}^{\tau U(n_1n_2+n_3n_4)} a_0^\dagger \mathrm{e}^{-\tau U(n_0n_3+n_5n_6)} a_4 a_4^\dagger a_0\rangle_0 + \langle \mathrm{e}^{\tau U(n_0n_3+n_5n_6)} a_4^\dagger \,\mathrm{e}^{-\tau U(n_1n_2+n_3n_4)} a_0 a_0^\dagger a_4\rangle_0 \\ &= \langle \mathrm{e}^{\tau U(n_1n_2+n_3n_4)} \mathrm{e}^{-\tau U n_5 n_6} a_0^\dagger a_4 a_4^\dagger a_0\rangle_0 + \langle \mathrm{e}^{\tau U(n_0n_3+n_5n_6)} \mathrm{e}^{-\tau U n_1 n_2} a_4^\dagger a_0 a_0^\dagger a_4\rangle_0 \end{aligned} \tag{21a}$$

where rule 1 has been used first and then rule 2. Using (2), one gets

$$2M(\tau) = \langle e^{\tau U(n_1n_2+n_3n_4)} e^{-\tau U n_5 n_6}(1-n_4)n_0\rangle_0 + \langle e^{\tau U(n_0n_3+n_5n_6)} e^{-\tau U n_1 n_2}(1-n_0)n_4\rangle_0$$
$$= \langle e^{\tau U n_1 n_2}\, e^{-\tau U n_5 n_6}(1-n_4)n_0\rangle_0 + \langle n_0 \leftrightarrow n_4, n_1 \leftrightarrow n_5, n_2 \leftrightarrow n_6\rangle_0 \tag{21b}$$

where the operator identity

$$f(n_i)(1-n_i) = f(0)(1-n_i), \quad (n_i = 0, 1) \tag{21c}$$

has been used. Now using rule 3 one obtains

$$2M(\tau) = \langle (1 - n_1n_2 + n_1n_2\, e^{\tau U})(1 - n_5n_6 + n_5n_6\, e^{-\tau U})(1-n_4)n_0\rangle_0$$
$$+ \langle n_0 \leftrightarrow n_4, n_1 \leftrightarrow n_5, n_2 \leftrightarrow n_6\rangle_0. \tag{21d}$$

Expanding within the (21*d*) thermal average symbols, gathering terms and exploiting kagomé lattice symmetry by equating geometrically equivalent correlations, one then substitutes the final expanded form of (21*d*) into (16*b*) yielding

$$M(\tau) = \frac{1}{2}(\langle a_0^\dagger(\tau)a_4(\tau)a_4^\dagger(0)a_0(0)]\rangle_0 + \langle a_4^\dagger(\tau)a_0(\tau)a_0^\dagger(0)a_4(0)]\rangle_0)$$
$$= \sum_{l=-1}^{1} e^{-l\tau U} P(l) \tag{22}$$

where the coefficients are given by

$$P(-1) = a_2 - x_4 - x_7 + x_{10} \tag{23a}$$

$$P(0) = a_1 - a_2 - x_1 - x_3 + 2(x_4 + x_7 - x_{10}) \tag{23b}$$

$$P(1) = x_3 - x_4 - x_7 + x_{10} \tag{23c}$$

with previously defined [1] thermal average notations (see figure 2)

$$\begin{aligned} &a_1 \equiv \langle n_0\rangle_0, \qquad a_2 \equiv \langle n_0n_1n_2\rangle_0, \\ &x_1 \equiv \langle n_0n_4\rangle_0, \qquad x_3 \equiv \langle n_0n_5n_6\rangle_0, \\ &x_4 \equiv \langle n_0n_1n_2n_4\rangle_0 = \langle n_0n_4n_5n_6\rangle_0, \\ &x_7 \equiv \langle n_0n_1n_2n_5n_6\rangle_0, \qquad x_{10} \equiv \langle n_0n_1n_2n_4n_5n_6\rangle_0. \end{aligned} \tag{24}$$

As a brief retrospective, the Wu seminal results [2] enable the grand canonical partition function of the unperturbed lattice-gas model $\mathcal{H}_0$ (6b) to be transformed into, aside from known prefactors, the magnetic canonical partition function of a standard honeycomb Ising model ferromagnet in a field. Pertinent solutions in (24) for the density $\rho = \langle n_0\rangle_0 \equiv a_1$ and elementary triplet correlation $\langle n_0n_1n_2\rangle_0 \equiv a_2$ could then be determined [1, 16] by logarithmic differentiations of the grand partition function with respect to $\beta\mu$ and $-\beta U$, respectively. The *a priori* knowledge of a_1, a_2 was instrumental in securing pertinent solutions for the remaining correlations $x_1, x_3, x_4, x_7, x_{10}$ in (24) by direct use of linear algebra methods [1].

Exact phase diagrams of the unperturbed system $\mathcal{H}_0$ are already known [16], viz, the liquid–vapor coexistence curve in density–temperature space (see figure 5) and the companion phase boundary curve in chemical potential-temperature space. Exact solutions are also known [1] for all thermal averages (24) along both the liquid and vapor branches of the coexistence curve of the unperturbed classical lattice gas system (Hamiltonian $\mathcal{H}_0$ in (1)) and along the continuation of the curvilinear diameter of its coexistence region into the disordered fluid region (see figure 5 in density–temperature space). It can therefore be suitably suggestive and

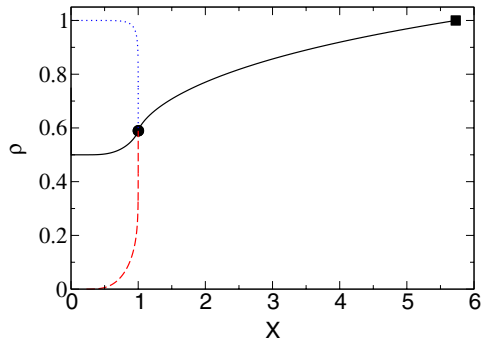

Figure 5. Liquid–vapor coexistence curve (dotted (blue) curve corresponding to the liquid branch and dashed (red) curve corresponding to the vapor branch) for the triplet interaction kagomé lattice gas [16] with unperturbed Hamiltonian $\mathcal{H}_0$ in (1). The colloidal particle number density is ρ and $x(= T/T_c)$ is the reduced temperature where $kT_c = |U|/3.96992\cdots$. The solid (black) curve is the curvilinear diameter of the coexistence region, beginning at zero temperature with $\rho = 1/2$ and ending at the critical point (solid circle) whose coordinates are $x = 1$, $\rho = \rho_c = 0.58931\cdots$. The extension of the curvilinear diameter into the disordered fluid region ends at the point (solid square) with coordinates $\rho = 1$, $x = 5.72739\cdots$. The companion liquid–vapor phase boundary, viz, chemical potential versus temperature, was also obtained in [16].

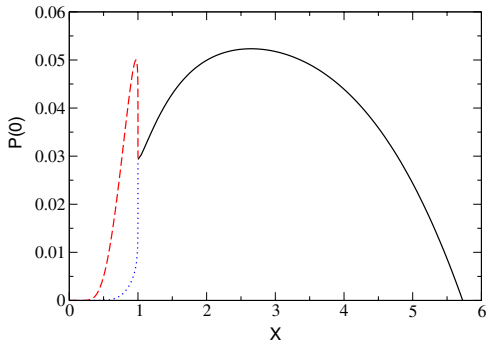

Figure 6. Temperature dependence of $P(0)$. The dashed (red) curve corresponds to the 'vapor' branch of the coexistence curve and the dotted (blue) curve corresponds to the 'liquid' branch. The solid (black) curve corresponds to the extension of the curvilinear diameter of the coexistence region into the disordered fluid region. The (reduced) temperature $x = T/T_c$ where the critical temperature T_c is given by $kT_c = |U|/3.96992\cdots$.

convenient to sometimes use the earlier [1] classical lattice gas language 'liquid' and 'vapor' as descriptions for the corresponding 'condensed' (or 'aggregated') and 'dilute' homogeneous phases of the unperturbed colloidal system $\mathcal{H}_0$.

Using (23), figures 6, 7 and 8 show resulting exact solutions along the above loci for $P(l)$, $l = 0$, 1 and -1, respectively, versus (reduced) temperature x. The form (22) reveals that $P(l)$ may be interpreted as the (unnormalized) probability of an ionic environment conducive to a 'hopping' event having energy change lU. A simple localized energy picture may clarify the concepts, at least heuristically. Using figure 2 site labels, assume an ion hops from site 0 to site 4. Letting triangles (012) $\equiv a$ and (346) $\equiv b$, their energies E_a and E_b can be either 0 or U. Then, hopping from energy $0 \to 0$ or $U \to U$ involves no energy transfer and thus relates to $P(0)$, while hopping from energy $U \to 0$ and $0 \to U$ relate to $P(+1)$ and $P(-1)$, respectively (see (33)). Note that triangle (034) is not considered since the hop from site 0 to

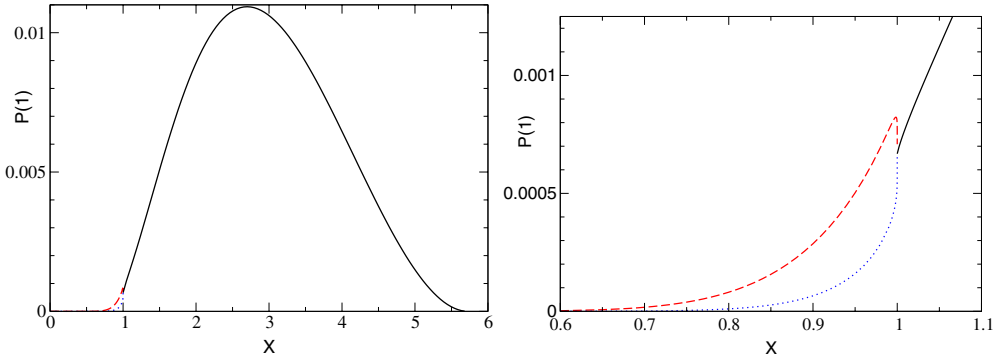

Figure 7. Left panel: temperature dependence of $P(1)$. Right panel: expanded view of $P(1)$ near the critical point. The dashed (red) curve corresponds to the 'vapor' branch of the coexistence curve and the dotted (blue) curve corresponds to the 'liquid' branch. The solid (black) curve corresponds to the extension of the curvilinear diameter of the coexistence region into the disordered fluid region. The (reduced) temperature $x = T/T_c$ where the critical temperature T_c is given by $kT_c = |U|/3.96992\cdots$.

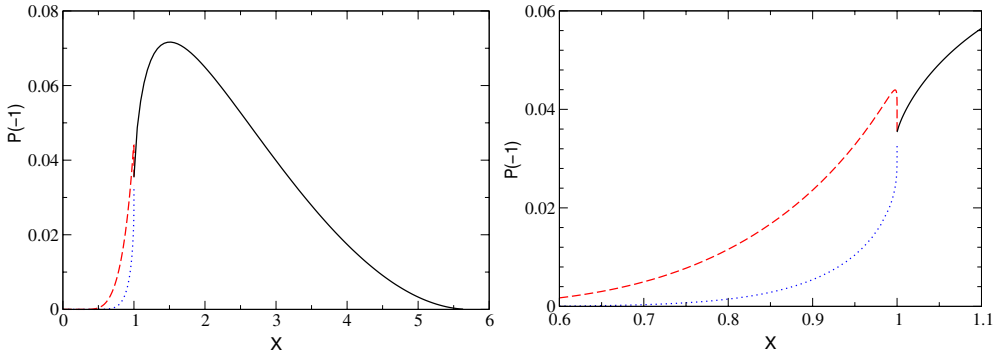

Figure 8. Left panel: temperature dependence of $P(-1)$. Right panel: expanded view of $P(-1)$ near the critical point. The dashed (red) curve corresponds to the 'vapor' branch of the coexistence curve and the dotted (blue) curve corresponds to the 'liquid' branch. The solid (black) curve corresponds to the extension of the curvilinear diameter of the coexistence region into the disordered fluid region. The (reduced) temperature $x = T/T_c$ where the critical temperature T_c is given by $kT_c = |U|/3.96992\cdots$.

site 4 does not alter its energy. Hence, as seen in the next section 7, only $P(0)$ is required for computing the dc ionic conductivity $\sigma_{\rm dc}$ whereas $P(-1), P(1)$ are also needed to compute the more general frequency-dependent ionic conductivity $\sigma(\omega)$.

The algebraic structures (23) of $P(l)$, $l = -1, 0, 1$, are significant. Each $P(l)$ is a linear combination of correlations with both positive and negative integer coefficients. Hence, there are *cancellation* effects, which make the *a priori* knowledge of *exact* solutions for thermal averages (24) crucial. One points out, e.g., that Boltzmann equation formulations cannot do justice in finding accurate information on multi-particle correlations since the Boltzmann equation is based upon a one-particle probability distribution. Furthermore, the linear combinations (23) of thermal averages provide the critical behavior of $P(l)$. Letting $\epsilon > 0$ be a small fractional deviation of temperature from its critical value, it is shown in

[1] that the familiar planar Ising critical singularities $\epsilon^{1/8}$ (algebraic branch point singularity of spontaneous magnetization) and $\epsilon \ln \epsilon$ (weak Ising energy-type singularity) characterize the critical behavior of the thermal averages (24) and thereby are inherent in $P(l)$ via (23). Thus, as $T \to T_c^-$, the long-range order (LRO) $\epsilon^{1/8}$-singularity dominates in $P(l)$ (note the corresponding infinite slopes in figures 6, 7, 8). As $T \to T_c^+$, only the weak energy-type singularity $\epsilon \ln \epsilon$ appears in $P(l)$ since LRO is identically zero in the disordered region.

Further remarks on the equilibrium phase diagram in figure 5 may be opportune. The length $\rho_l - \rho_v$ of a vertical (isotherm) tie-line connecting points on the liquid and vapor branches of the coexistence curve is the value of the LRO parameter in the fluid system at the select temperature, and the arithmetic mean $\frac{1}{2}(\rho_l + \rho_v)$ locates the mid-point of the vertical tie-line. Then the *diameter* of the coexistence region may be viewed as the loci of mid-points of the vertical tie-lines spanning the complete coexistence region. The concave-upward *curvilinear diameter* in figure 5 is an indicator of the *asymmetric* shape of the rounded coexistence curve for the current attractive *three-particle* interaction Hamiltonian $\mathcal{H}_0$ (6b), contrasting the constant rectilinear (i.e., straight) diameter and associated *symmetric* shape of the rounded coexistence curve for a conventional planar lattice gas model with attractive nearest-neighbor *pair* interactions. In figure 5, the extension of the curvilinear diameter into the disordered fluid region is the continuing sigmoidal curve [1, 16] which is monotonically increasing and concave downward, eventually terminating (solid square). The behavior again contrasts the conventional case of pair interactions wherein the extension of the constant rectilinear diameter into the disordered region continues indefinitely.

7. Initial dynamic ionic conductivity $\sigma(\omega)$

The Matsubara (thermal) bosonic Green functions, e.g., $\Pi(\tau) = \frac{1}{2}\langle T_\tau \mathcal{J}(\tau) \cdot \mathcal{J}(0)\rangle_H$, are defined as a function of τ with domain

$$-\beta \leqslant \tau \leqslant \beta \tag{25}$$

and possess the periodic property

$$\Pi(\tau + \beta) = \Pi(\tau), \qquad \text{for} \quad -\beta < \tau < \beta. \tag{26}$$

Consequently, $\Pi(\tau)$ may be expanded into a complex Fourier series as

$$\Pi(\tau) = \frac{1}{\beta} \sum_{n=-\infty}^{\infty} \mathrm{e}^{-\mathrm{i}\omega_n \tau} \Pi(\mathrm{i}\omega_n), \tag{27a}$$

$$\Pi(\mathrm{i}\omega_n) = \int_0^\beta \mathrm{d}\tau\, \mathrm{e}^{\mathrm{i}\omega_n \tau} \Pi(\tau), \tag{27b}$$

where

$$\omega_n = \frac{2\pi n}{\beta}, \qquad n = 0, \pm 1, \pm 2, \ldots. \tag{27c}$$

Using (16*a*) and (22), the (thermal) Matsubara Green function in zeroth order approximation for the present problem becomes

$$\Pi(\tau) = R \sum_{l=-1}^{1} P(l)\, \mathrm{e}^{-l\tau U} \tag{28a}$$

where the constant prefactor

$$R \equiv \frac{\mathcal{N}\tilde{z}}{2} \left(\frac{q t_0 d}{\hbar}\right)^2. \tag{28b}$$

Substituting (28*a*) into (27*b*) gives

$$\Pi(\mathrm{i}\omega_n) = R\sum_l P(l)\int_0^\beta \mathrm{d}\tau\, \mathrm{e}^{(\mathrm{i}\omega_n - lU)\tau}$$
$$= R\sum_l P(l)\,\frac{\mathrm{e}^{-lU\beta}-1}{\mathrm{i}\omega_n - lU}. \tag{29}$$

Expression (29) illustrates the general property that the Fourier transform $\Pi(\mathrm{i}\omega_n)$ of the thermal (Matsubara) Green function $\Pi(\tau)$ is only found at a denumerably infinite set of points along the imaginary 'frequency' axis, i.e., at points $\mathrm{i}\omega_n$, $n = 0, \pm1, \pm2, \ldots$ (so-called *Matsubara frequencies* ω_n). The analytic continuation of $\Pi(\mathrm{i}\omega_n)$ from the infinite discrete set of points on the imaginary axis to the entire upper-half complex plane is simply achieved by replacing $\mathrm{i}\omega_n$ by z in (29), yielding

$$\Pi(z) = R\sum_l P(l)\,\frac{\mathrm{e}^{-lU\beta}-1}{z - lU}. \tag{30}$$

The analytic continuation (30) of the Matsubara (thermal) Green function is important since it enables one to immediately obtain the temporal Fourier transform of the physical two-time retarded Green function. Specifically, one can prove the mapping [15]

$$\Pi(\hbar\omega + \mathrm{i}\epsilon) = \Pi_{\text{retarded}}(\omega), \tag{31}$$

where ϵ is a positive infinitesimal.

Although linear response theory and the Kubo formula are developed using the two-time retarded Green functions, one can easily transcribe the results, using (31), into the language of thermal (Matsubara) Green functions. As an example, the real part of the conductivity, for an isotropic planar specimen of area A, is then given using the Kubo formula as

$$\sigma(\omega) = \frac{1}{A\omega}\mathrm{Im}\left[\lim_{\epsilon\to0}\Pi(\hbar\omega + \mathrm{i}\epsilon)\right]. \tag{32}$$

For the present problem, one substitutes (30) into (32) which gives

$$\sigma(\omega) = \frac{1}{A\omega}\mathrm{Im}\left[\lim_{\epsilon\to0} R\sum_l P(l)\,\frac{\mathrm{e}^{-lU\beta}-l}{\hbar\omega - lU + \mathrm{i}\epsilon}\right]$$
$$= \frac{\pi R}{A}\,\frac{1-\mathrm{e}^{-\beta\hbar\omega}}{\omega}\sum_l P(l)\,\delta(\hbar\omega - lU)$$
$$= \frac{\pi R}{A}\,\frac{1-\mathrm{e}^{-\beta\hbar\omega}}{\hbar\omega}\sum_l P(l)\,\delta\left(\omega - \frac{lU}{\hbar}\right), \tag{33}$$

where use has been made of the symbolic identity

$$\lim_{\epsilon\to0}\frac{1}{x - x_0 \pm \mathrm{i}\epsilon} = \mathrm{P}\,\frac{1}{x - x_0} \mp \mathrm{i}\pi\delta(x - x_0) \tag{34a}$$

with the symbol P representing the Cauchy principal value, and lastly utilizing the Dirac δ-function property

$$\delta(ax) = \frac{1}{a}\delta(x). \tag{34b}$$

The delta-functions in (33) are expected to be 'smeared out' and become finite peaks due to the scattering between the mesoscopic colloidal ions and the microscopic particles of the solvent. Also, it can be shown [15] that $\sigma(\omega) = \sigma(-\omega)$ which implies, using (33), that $P(l) = \mathrm{e}^{\beta lU}P(-l)$. Thus $P(1)$, $P(-1)$ are functionally dependent, with $P(1) < P(-1)$ for finite temperatures (since $U < 0$), which agrees with figures 7 and 8.

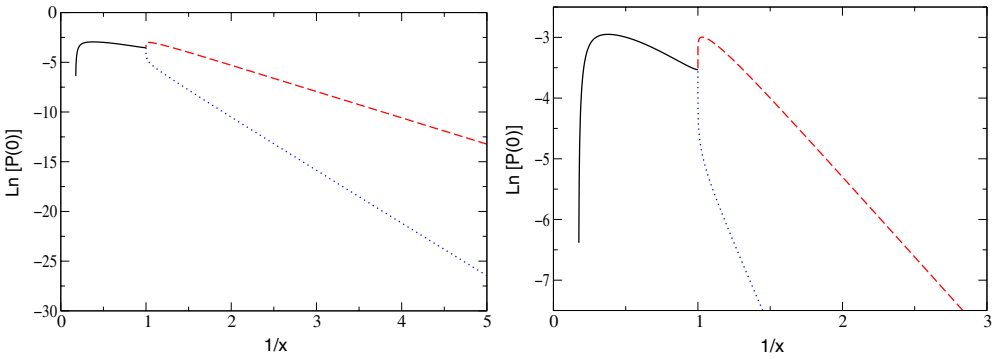

Figure 9. Arrhenius behavior of the dc conductivity $\sigma_{\rm dc}$. Left panel: logarithm of $P(0)(=\sigma_{\rm dc}T/C)$ as a function of the inverse (reduced) temperature. Right panel: expanded plot of logarithm of $P(0)$ near the critical point. The dashed (red) curve corresponds to the 'vapor' branch of the coexistence curve and the dotted (blue) curve corresponds to the 'liquid' branch. The solid (black) curve corresponds to the extension of the curvilinear diameter of the coexistence region into the disordered fluid region. The (reduced) inverse temperature $1/x = T_c/T$ where the critical temperature T_c is given by $kT_c = |U|/3.96992\cdots$.

In particular, the dc ionic conductivity is given by, using (33) and (28*b*),

$$\sigma_{\rm dc} \equiv \lim_{\omega\to 0}\sigma(\omega) = \frac{\pi R}{A}\beta P(0)\delta(\omega)$$
$$= \frac{2\pi\mathcal{N}}{AkT}\left(\frac{qt_0 d}{\hbar}\right)^2 P(0)\delta(\omega) \tag{35}$$

having substituted the kagomé lattice coordination number $\tilde{z} = 4$ and the static limit results

$$\lim_{\omega\to 0}\frac{1-{\rm e}^{-\beta\hbar\omega}}{\hbar\omega} = \beta; \quad \lim_{\omega\to 0}\sum_l P(l)\,\delta\left(\omega - \frac{lU}{\hbar}\right) = P(0)\delta(\omega). \tag{36}$$

Summarizing, (35) yields

$$\sigma_{\rm dc}T = CP(0) \tag{37a}$$

where $P(0)$ was given previously by (23*b*) and is known exactly along select loci in density–temperature space. The coefficient

$$C \equiv \frac{2\pi\mathcal{N}}{Ak}\left(\frac{qt_0 d}{\hbar}\right)^2\delta(\omega)$$
$$= \sqrt{3}\,\frac{\pi}{k}\left(\frac{qt_0}{\hbar}\right)^2\delta(\omega), \tag{37b}$$

having lastly used the geometrical constant $\mathcal{N}d^2/A = \sqrt{3}/2$ for the kagomé lattice.

8. Arrhenius behavior of dc ionic conductivity $\sigma_{\rm dc}$

Figure 9 exhibits a semi-log plot of the dc ionic conductivity result (37), where the delta-function in C has been suppressed (later, the delta-function is replaced [13] by the inverse of a 'relaxation frequency'). Specifically, one initially charts $\ln(\sigma_{\rm dc}T/C)$ versus (reduced) inverse temperature $1/x$, or equivalently, $\ln P(0)$ versus $1/x$. The straight-line segments in figure 9 show clear Arrhenius behaviors over a wide range of temperature along the 'liquid'

and 'vapor' branches, resulting from the exact solution for $P(0)$. This suggests that, because of the competing correlations, each ion feels an effective single-particle potential. The disordered fluid phase also seems to have an Arrhenius form, albeit over a smaller range. The negative *slopes* $\tilde{\Delta}_l$ (liquid branch), $\tilde{\Delta}_v$ (vapor branch) $\tilde{\Delta}_d$ (disordered fluid) of the corresponding straight line segments in figure 9 will directly lead to the characteristic *static activation energies* Δ_l, Δ_v, Δ_d in the dc ionic conduction process. More particularly,

$$\tilde{\Delta}_l = -5.3, \qquad \tilde{\Delta}_v = -2.6, \qquad \tilde{\Delta}_d = -1.1 \tag{38}$$

along, respectively, the liquid (blue dotted) and vapor (red dashed) branches of the coexistence curve and the (solid line) trajectory in the disordered fluid region of figure 9. The latter trajectory eventually bends downward due to the 'overloading' of ions (or dearth of vacancies required for hopping) leading to $\sigma_{\rm dc} \to 0$ as $\langle n_0 \rangle \to 1$.

In a standard Arrhenius exponential form, the positive ratio Δ/k is reckoned using a $1/T$ abscissa rather than $1/x(= T_c/T)$. Hence, simple rescaling of $|\tilde{\Delta}_l|$, $|\tilde{\Delta}_v|$, $|\tilde{\Delta}_d|$ in (38) gives the activation energies Δ_l, Δ_v, and Δ_d as

$$\Delta_l = kT_c|\tilde{\Delta}_l| = 1.3|U|, \qquad \Delta_v = kT_c|\tilde{\Delta}_v| = 0.6|U|, \qquad \Delta_d = kT_c|\tilde{\Delta}_d| = 0.28|U| \tag{39}$$

having substituted the critical constant [1] $kT_c = |U|/\ln[(2+\sqrt{3})^3 + 1] = |U|/3.96992\cdots$. In summary, along the straight line segments in figure 9,

$$\begin{aligned} \sigma_{\rm dc} &\approx C\frac{{\rm e}^{-1.3|U|/kT}}{T}; && \text{liquid branch} \\ &\approx C\frac{{\rm e}^{-0.6|U|/kT}}{T}; && \text{vapor branch} \\ &\approx C'\frac{{\rm e}^{-0.28|U|/kT}}{T}; && \text{disordered fluid trajectory} \end{aligned} \tag{40}$$

where C is given by (37*b*) and $C' = {\rm e}^{-2.5}C$ since the associated straight-line segment in figure 9 shows a y-axis intercept value -2.5. Equation (40) suggests that the three-body interaction strength $|U|$ could also be obtained experimentally from the temperature dependence of the dc conductivity, away from the critical point, along either branch of the coexistence curve thereby avoiding critical fluctuations.

9. Experimental considerations

Although speculative to some degree, it may prove valuable to suggest and discuss a possible application of the theory. As mentioned in the introduction, we have in mind a 'Konstanz–Stuttgart' type of ionic system considered in [10], where it was shown that by screening away the two-particle interactions using appropriate solvents, it is possible to achieve a system of 'mesoscopic' charged silica spheres suspended in water at room temperature where three-particle *attractive* interactions dominate. Although the experiment was done in a bulk system, it should be possible to inject the suspension into a thin cell to achieve an effectively two-dimensional system. Our two-dimensional quantum lattice liquid model upon a triangular or kagomé lattice structure will then capture the essentials of a system with highly localized three-body interactions. For the present attractive interactions, and since the lattice parameter d disappears from the expression for C in (37b), the results are expected to be insensitive to the details of the close-packed lattice chosen, and our choice of the kagomé lattice allows us to include the multi-particle correlations *exactly* in the present theory.

In such a system, the aggregation phase transitions and criticality directly involve the *ordering* degrees of freedom associated with the ionic silica spheres, while the *non-ordering*

degrees of freedom are associated with the water molecules and counterions. The proposed model Hamiltonian $\mathcal{H}$ in section 2 explicitly contains only the ordering degrees of freedom. This means that much of the complexity associated with a generic system with repulsive two-particle interactions is not included in our model. However, in the present work we restrict ourselves in evaluating only the *anomalous* part of the conductivity, namely, the additional contribution due to the existence of the phase transition. Although the non-ordering degrees of freedom remain important for the background total conductivity, they do not contribute to possible anomalies in the dc conductivity $\sigma_{\rm dc}$ along the coexistence curve or the finite-jump discontinuities in $\sigma_{\rm dc}$ upon crossing the phase boundary curve, except for a renormalization of the parameters that are relevant for the ordering itself. Thus in $\mathcal{H}$, the strength parameters $|U|$, t_0 of the potential and kinetic energies, respectively, should be considered as 'effective' parameters implicitly containing effects of the non-ordering degrees of freedom. These parameters $|U|$, t_0 can be eventually obtained by comparison with experiment. Specifically, $|U|$ is first found from the experimental value of the critical temperature and direct use of an exact critical constant. Then, t_0 is found as some fraction of $|U|$ by the most favorable fit between the theory and experiment over the entire relevant temperature range. Implementing the fundamental statistical theory of linear response (fluctuation-dissipation theorem), the model Hamiltonian $\mathcal{H}$ patently commands leading importance in the derivation and evaluation of the Kubo formula for the dynamic ionic conductivity of the charged silica spheres near their (aggregation) phase transitions.

With an attractive interaction, the model predicts a discontinuous phase transition across the liquid–vapor phase boundary and a continuous transition at a critical temperature [1, 16]. It is unclear whether the parameters in the room temperature experiments of [10] can be chosen, as temperature is lowered, in such a way that the onset (critical point) of equilibrium aggregation occurs before the salted water freezes. Nevertheless, it seems plausible that, perhaps in a cleverly designed variant of the above experiment, such a transition should be observable in the case of the silica or similar mesoscopic spheres, where condensation into clusters could be induced, e.g. by tuning the salinity of the solvent and lowering temperature [11]. Thus, the system could be prepared near a discontinuous phase transition, with a disordered fluid region at high temperatures and, at low temperatures, a heterogeneous mixture of a 'vapor' phase corresponding to the more mobile silica spheres and a 'liquid' phase corresponding to the clusters.

A major difficulty in a direct comparison of the theoretical predictions with experiments is that experiments are typically done at a fixed density, while our results are valid along the coexistence curve where exact correlations for the three-body interactions are known [1]. For example, in the low temperature mixed phase, the conductivity was calculated only along the coexistence curve and not inside the mixed phase. However, since the density on the coexistence curve is accurately known as function of temperature (see figure 5), it should be possible to prepare the sample at several specific density–temperature points.

Another inherent problem in a quantitative comparison between theory and experiment is the presence of the delta-function in (37*b*). As mentioned before, the delta-function is expected to be 'smeared out' due to scattering between the mesoscopic colloidal ions and the microscopic particles of the solvent. The background solvent and viscosity have not been incorporated into the present theory at a microscopic level. Hence, in the model Hamiltonian (1) for the colloidal ions, the parameters U, t_0 should be interpreted as 'effective' parameters describing the complete multi-component system. In general, the broadening of the delta function should include the transport time of a single silica sphere through the solvent. This would depend on the hydrodynamics of the solvent, but should be largely independent of the multiparticle correlations. The fact that the multiparticle correlations result in an Arrhenius

behavior implies that each ion feels an effective single particle potential with a barrier height given by the activation energy (39). This suggests that the temperature dependence of the transport time would be governed by the inverse of an effective 'relaxation frequency' ω_0 rather than by the mobility of the colloidal ions in the solvent. Note that the T-dependence arising from the hydrodynamics of the solvent is expected to be the same for pair and triplet interactions, while the T-dependence from $P(0)$ contains the special influence of the three-body attractive interactions that we are primarily interested in. In any case, additional T-dependence from the hydrodynamics of the solvent should be separately and directly measurable in a system with only a few ions and can be incorporated phenomenologically into the current theory.

Assuming that the delta-function can be replaced by the inverse of an effective 'relaxation frequency' ω_0 [13], the dc conductivity given by (37) can be written as

$$\begin{aligned}\sigma_{\rm dc} &\sim \sqrt{3}\pi \frac{1}{kT}\left(\frac{qt_0}{\hbar}\right)^2 \frac{P(0)}{\omega_0} \\ &= \sqrt{3}\pi \frac{e^2}{\hbar}\left(\frac{q}{e}\right)^2 \frac{t_0^2}{(kT)(\hbar\omega_0)} P(0). \end{aligned} \tag{41}$$

For definiteness, we assume that the relaxation frequency is related to the average thermal energy, such that $\hbar\omega_0 \sim kT$ [13]. As a crude estimate, at $T \sim T_c \cong |U|/4k \sim 30\,\mathrm{K}$,[4] this means that $\omega_0 \sim 3 \times 10^{12}\ \mathrm{s}^{-1}$, which is consistent with typical optical frequencies ($10^{13}\ \mathrm{s}^{-1}$) observed in simple solids [18]. Then (41) becomes

$$\begin{aligned}\sigma_{\rm dc} &\sim \sqrt{3}\pi \frac{e^2}{\hbar}\left(\frac{q}{e}\right)^2 \left(\frac{t_0}{kT}\right)^2 P(0) \\ &= \sqrt{3}\pi \frac{e^2}{\hbar}\left(\frac{q}{e}\right)^2 \left(\frac{t_0}{|U|}\right)^2 \left(\frac{|U|}{kT_c}\right)^2 \left(\frac{T_c}{T}\right)^2 P(0) \\ &= \tilde{C}\left(\frac{T_c}{T}\right)^2 P(0) \end{aligned} \tag{42a}$$

where we have used $kT_c \cong |U|/4$ for our model and defined $\alpha \equiv t_0/|U|$ yielding

$$\tilde{C} = \sqrt{3}\ 16\pi\alpha^2 \frac{e^2}{\hbar}\left(\frac{q}{e}\right)^2. \tag{42b}$$

Here $e^2/\hbar = 2.4 \times 10^{-4}\Omega^{-1}$ is the quantum unit of conductance and $\alpha \ll 1$ is necessary for our perturbation theory to remain valid.

Equation (42*a*) describes the predicted temperature dependence of the dc ionic conductivity. Figure 10 plots the dimensionless conductivity

$$\eta \equiv \frac{\sigma_{\rm dc}}{\tilde{C}} = \frac{P(0)}{(T/T_c)^2} \tag{43}$$

as a function of the reduced temperature $x = T/T_c$. As mentioned earlier, the ionic conductivity in the mixed phase will be dominated by contributions from the 'vapor' phase, and an experiment may observe an increase in conductivity by almost a factor of two when the temperature is decreased from $T = T_c$ ($\eta \sim 0.03$) to $T = 0.9T_c$ ($\eta \sim 0.056$).

We note that while the explicit $1/T$ dependence in equation (41) results from precise calculations, our assumption that the relaxation frequency $\hbar\omega_0 \sim kT$ is responsible for the explicit $1/T^2$ dependence in equation (42*a*). While the assumption seems reasonable, the non-ordering degrees of freedom not included in the current theory could result in a different

[4] Note that while T_c is related to the 'bare' interaction parameter $|U|$ [1], we use the 'dressed' value of $|U|$ measured in the room-temperature experiment [10]. Allowing for the difference would typically increase the value of T_c.

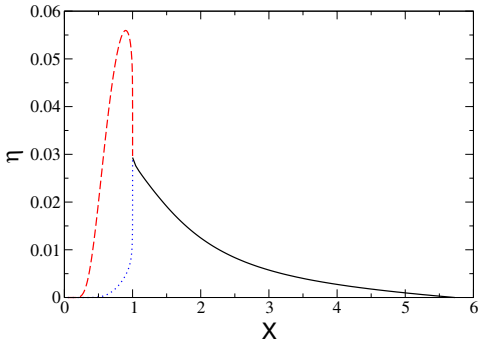

Figure 10. Dimensionless ratio $\eta = \sigma_{\rm dc}/\tilde{C} = P(0)/x^2$ as a function of the (reduced) temperature $x = T/T_c$. The dashed (red) curve corresponds to the 'vapor' branch of the coexistence curve and the dotted (blue) curve corresponds to the 'liquid' branch. The solid (black) curve corresponds to the extension of the curvilinear diameter of the coexistence region into the disordered fluid region. The critical temperature T_c is given by $kT_c = |U|/3.96992\cdots$. The dashed (red) curve attains a narrow maximum having coordinates $x_{\rm max} = 0.90\cdots$, $\eta_{\rm max} = 0.056\cdots$, associated with a low density coordinate $\rho_{\rm max} = 0.12\cdots$ in figure 5.

effective temperature dependence of ω_0. However, this may be obtained from a comparison of the theoretical plot with the experimental temperature dependence of the dc-conductivity in the region where $\sigma_{\rm dc}$ is dominated by the explicit power-law behavior. In that context, one should leave $\omega_0(T)$ as an unknown function and obtain it experimentally by fitting the conductivity in the appropriate temperature regime.

Using (42), we can also estimate the magnitude of the conductivity if we assume a crude value for the hopping parameter α. The effective charge q on the silica spheres in the experiment was reported to be $q/e = 6500$. Then the maximum conductivity, at $x = 0.9$, is given by

$$\sigma_{\rm dc} \sim 5 \times 10^4\ \alpha^2\ \Omega^{-1}. \tag{44}$$

Thus, even with a small hopping parameter $\alpha > 5 \times 10^{-3}$, the conductivity can be comparable or larger than the superionic conductivity ($\sigma_{\rm dc} \sim 0.3\ (\Omega{\rm cm})^{-1}$) observed in layered $AgCrS_2$ just above its order–disorder phase transition temperature [17]. It should also be possible to increase α by, e.g., reducing the mass and size of the silica spheres. If realized, the anomalously large ionic conductivities could have implications in advanced battery and fuel cell technologies.

In figure 10, the lengths $\eta_v - \eta_l$ of the vertical tie-lines spanning the coexistence region equal, as usual, the corresponding finite-jump discontinuities in η upon crossing the *companion* phase boundary curve ($\mu/|U|$ versus x). The finite-jump discontinuity $\Delta\eta$ vanishes continuously at both the absolute zero and critical temperatures, and attains a narrow maximum at $x_{\rm max} \approx 0.90$. The measurable $\Delta\eta$ is fully attributable to the presence of the (aggregation) phase transitions.

In the concluding comments of [10], three regions of colloidal particle density are focused upon, viz, (i) low, (ii) intermediate and (iii) high densities. Relative weight considerations are argued for the influence of multiparticle interactions in each of the density regions. Specifically, one reasons in [10] that pair interactions outweigh triplet interactions in (i), both pair and triplet interactions need attention in (ii), and pair, triplet and higher-order interactions are concerns in (iii). In the context of the current paper, if salt is aptly added to the water solvent, the electrostatic pair interactions between the mesoscopic ions are screened.

Hence, one can consider their triplet interactions to govern the (i) and (ii) density regions, and recall that the anomalously large η-peak in figure 10 arises in the low density region (i). In the remaining region (iii) of high density, the effects of the higher-order multiparticle interactions are unknown. However, if one conjectures that there exists an *ordering of strengths* among the multiparticle interactions, say, three-particle stronger than four-particle stronger than five-particle and so forth, then higher-order multiparticle interactions would presumably produce small or negligible effects compared to the dominant triplet interactions. In any event, the collective effects of the higher-order n-particle ($n > 3$) interactions at high densities could conceivably be inferred from meticulous comparisons of experiments with the present ($n = 3$) theoretical results.

10. Summary and discussion

A system of charged mesoscopic particles with dominant three-particle interaction was modeled by a quantum lattice liquid on the planar kagomé lattice. The two-parameter Hamiltonian contained a classical potential energy form of attractive three-particle interactions around elementary triangles of the lattice, and the kinetic energy form contained hopping-type terms along nearest neighbor bonds. The method employed to theoretically investigate ionic conductivity for 'weak hopping' developed a quantum many-body perturbation expansion of the thermal (Matsubara) Green function (current–current correlation). The ionic conductivity was calculated using the Kubo formula, more particularly, the frequency-dependent conductivity was obtained from the imaginary part of the Fourier transform of the two-time retarded Green function which in turn was found from the analytic continuation and mapping of the Matsubara Green function. As results, Arrhenius relations were revealed in zeroth-order approximation for the dc ionic conductivity $\sigma_{\rm dc}$ along both the 'liquid' and 'vapor' branches of the unperturbed system coexistence curve (except in close proximity to the critical point) and along the continuation of its curvilinear diameter into the disordered fluid region (except in close proximity to full occupancy of the lattice). The Arrhenius plots directly yielded static activation energies along the above trajectories in density–temperature space. Experimental possibilities relating to $\sigma_{\rm dc}$ and equilibrium aggregation were discussed.

To assess the effects of higher-order perturbation terms upon the present zeroth-order results, one recognizes at the outset that the first-order perturbation contributions for the close-packed kagomé lattice are α^3-terms (closed directed diagrams around elementary triangles). If the smallness parameter $\alpha \equiv t_0/|U| \ll 1$ (weak hopping), the quantitative effects of the higher-order α^3-terms are expected to be small compared to the current zeroth-order α^2-terms. A more definitive and overall assessment awaits further explicit perturbation calculations and experimental data.

In perturbation theory, one usually chooses an unperturbed part having exactly known solutions. The discretization of configurational continuum space offers special advantages in this regard. Most exact solutions for correlations, phase transitions and critical/multicritical phenomena are found in two-dimensional lattice-statistical models. Indeed, exact solutions were needed and are known in the kagomé lattice unperturbed Hamiltonian $\mathcal{H}_0$ (1) for use in the quantum many-body perturbation expansion of the Matsubara Green function. Limitations relating to the discretization of continuum space appear at wavelengths comparable or smaller than the lattice spacing. However, the present work does not consider the wave-vector dependent ionic conductivity $\sigma(\vec{k}, \omega)$. More specifically, one only considers the long-wavelength *hydrodynamic limit* $k \to 0$ associated with the *uniform* electric field stimulus.

In charged colloidal systems, experimental possibilities for phase transitions and critical phenomena exist. If there is a predominant attraction, the mesoscopic ionic particles will

aggregate or condense into clusters. This can be induced, e.g., by adding salt to the solvent to screen the electrostatic repulsive pair interactions between colloidal ions, or by adding a polymer which acts as a depletion agent for tuning the salinity. As stated earlier, the model parameters U, t_0 in the present theory are adjustable parameters and are found *a posteriori* by comparison with experiments. More particularly, U is first acquired from the experimental critical temperature T_c using the exact critical constant [1] $\beta_c|U| = 3.96992\cdots$, $\beta_c = 1/kT_c$. Then t_0 is obtained as some fraction of $|U|$ by the most favorable fit between the theory and experiment for $\sigma_{\rm dc}$ over the entire relevant temperature range.

One can speculate whether the present two-dimensional model with its mathematical feasibility and results could have wider generic relevance than in thin films. Insights and guidance in similar three-dimensional colloidal systems assuredly remain a possibility, and hold special appeal since conductivity in three dimensions generally exceeds that in two dimensions. Typically, in contrast to mesoscopic ions, screening the electrostatic pair interactions between microscopic ions is problematical so multi-particle interaction effects are most often perturbative rather than dominant. On the other hand, pair interactions between cold polar molecules in an optical lattice driven by microwave fields can be tuned out by an external field, leaving a dominant three-body interaction [6]. Such a system could be modeled by a generalized Hubbard Hamiltonian with three-particle interactions [6]. Our model, which precludes double occupancy, will then correspond to an infinite on-site repulsion in the Hubbard model. For typical single-species insulating (nonionic) fluids, the dominant microscopic interactions are given by the Lennard–Jones 6–12 pair potential, along with short-range weak repulsive triplet interactions of Axilrod–Teller type [19]. Nevertheless, it seems imprudent to discount the possibility for discovery or developments of novel and diverse systems possessing predominant three-particle interactions that are both highly localized and attractive.

Acknowledgment

The authors wish to express their gratitude to C Bechinger for valuable correspondence concerning his experiments on charged colloidal suspensions.

References

[1] Barry J H, Muttalib K A and Tanaka T 2008 *Phys. Rev.* E **77** 011102
[2] Wu F Y 1974 *J. Math. Phys.* **15** 687
Wu X N and Wu F Y 1988 *J. Stat. Phys.* **50** 41
Wu X N and Wu F Y 1989 *J. Phys. A: Math. Gen.* **22** L55
Wu X N and Wu F Y 1989 *J. Phys. A: Math. Gen.* **22** L1031
Wu F Y and Wu X N 1989 *Phys. Rev. Lett.* **63** 465
Wu F Y 1990 *J. Phys. A: Math. Gen.* **23** 375
[3] For a review, see Roger M, Hetherington J H and Delrieu J M 1983 *Rev. Mod. Phys.* **55** 1
[4] Eccleston R S, Uehara M, Akimitsu J, Eisaki H, Motoyama N and Uchida S I 1998 *Phys. Rev. Lett.* **81** 1702
Coldea R, Hayden S M, Aeppli G, Perring T G, Frost C D, Mason T E, Cheong S-W and Fisk Z 2001 *Phys. Rev. Lett.* **86** 5377
Nunner T S, Brune P, Kopp T, Windt M and Grüninger M 2002 *Phys. Rev.* B **66** 180404
Schmidt K P and Uhrig G S 2005 *Mod. Phys. Lett.* B **19** 1179
Notbohm S *et al* 2007 *Phys. Rev. Lett.* **98** 027403
[5] Pachos J K and Plenio M B 2004 *Phys. Rev. Lett.* **93** 056402
[6] Büchler H P, Micheli A and Zoller P 2007 *Nature Phys.* **3** 726
Schmidt K P, Dorier J and Läuchli A M 2008 *Phys. Rev. Lett.* **101** 150405
[7] Hafner J 1987 *From Hamiltonians to Phase Diagrams* (Berlin: Springer)
[8] Österlund L, Pedersen M O, Stensgaard I, Laegsgaard E and Besenbacher F 1999 *Phys. Rev. Lett.* **83** 4812

[9] Ovchinnikov M and Apkarian V A 1999 *J. Chem. Phys.* **110** 9842
[10] Dobnikar J, Brunner M, Grünberg H-H von and Bechinger C 2004 *Phys. Rev.* E **69** 031402
[11] Bechinger C 2011 private communication
[12] Matsubara T and Matsuda H 1956 *Prog. Theor. Phys.* **16** 569
Matsubara T and Matsuda H 1957 *Prog. Theor. Phys.* **17** 19
[13] Mahan G D 1976 *Phys. Rev.* B **14** 780
[14] Tanaka T, Sharma N L, Munera C H and Barry J H 1982 *App. Surf. Sci.* **11/12** 605
Sharma N L and Tanaka T 1983 *Phys. Rev.* B **28** 2146
Tanaka T, Sawtarie M A, Barry J H, Sharma N L and Munera C H 1986 *Phys. Rev.* B **34** 3773
[15] Abrikosov A A, Gorkov L P and Dzyaloshinski J E 1963 *Methods of Quantum Field Theory in Statistical Physics* (Englewood Cliffs, NJ: Prentice-Hall)
Abe R 1975 *Statistical Mechanics* (Tokyo: University of Tokyo Press)
Mahan G D 1981 *Many-Particle Physics* (New York: Plenum Press)
Bruus H and Flensberg K 2004 *Many-Body Quantum Theory in Condensed Matter Physics* (Oxford: Oxford University Press)
[16] Barry J H and Sullivan N S 1993 *Int. J. Mod. Phys.* B **7** 2831
[17] Hibma T 1980 *Solid State Commun.* **33** 445
[18] Kittel C 1971 *Introduction to Solid State Physics* 4th edn (New York: Wiley)
[19] Axilrod B M and Teller E 1943 *J. Chem. Phys.* **11** 299